Liner Load Estimation for Soft Ground Pressure Balance TBM Shield Tunnel Projects

Tamir Epel, Mike Mooney, Marte Gutierrez
Colorado School of Mines

ABSTRACT

Pressure balance TBM tunneling has advanced to the point where it is routine to essentially match the face and annulus pressures around the TBM envelope. Resulting ground deformations are sensitive to the face pressure-effective stress ratio. The loading on segmental lining is impacted by this, and specifically the degree of pre-convergence, i.e., the relaxation and arching of the ground prior to lining installation. With very little information on the convergence-confinement relationship in pressure-balance TBM situations. This paper addresses the loading on precast segmental lining during pressure balance TBM tunneling based on lining load data from the Northgate Link project.

Key words: Segmental lining design, pressure balance TBM, Convergence confinement method, Twin tunnels.

INTRODUCTION

Liner load estimation in pressure balance TBM tunneling (using both EPB and slurry machines) is highly dependent on the degree of pre-convergence prior to the installation of the segmental lining rings. The load redistribution concept is commonly taken into account in tunnel lining design by the use of the convergence-confinement method (CCM). More commonly used in conventional tunneling, the CCM is used in 2D analysis to account for the 3D effects of the excavation face, allowing for pre-convergence in front and behind the tunnel face, prior to lining installation. The pre-convergence allowed in this method results in more realistic lower liner loads as the ground stresses are redistributed and are partly taken by the ground. To implement the 3D effects in 2D numerical analysis several approaches are commonly used as: the contraction method, the stress reduction method, and the grout pressure method.

While in conventional tunneling, the geostatic stresses are not balanced at the face of excavation and at the tunnel periphery for a short time after excavation. In pressure balance TBM tunneling, the face and excavation boundary are supported by pressurized slurry or conditioned muck to reduce surface settlements. The allowance of pre-convergence prior to liner placement accomplished through the CCM is widely used for conventional tunneling. However, in most design processes involving pressurized shield tunneling projects, pre-convergence is often neglected. The rationale is that pressure at the face of the excavation reduces the pre-convergence, and that the assumption of zero pre-convergence yields more conservative (higher) lining forces.

In this paper, data from strain gages installed in segmental lining rings on the Seattle Sound Transit Northlink tunnel project (Frank et al. 2015, Epel et al. 2018a, Epel. et al. 2018b) are analyzed during the final state of geostatic loading in varying geologies along the glacially-deposited alignment. Commonly used numerical modeling methodologies are employed to predict liner loading. The experimental and model results are compared.

PROJECT BACKGROUND

The Northgate link extension project includes 5.6 km of twin bored tunnels and 23 cross passages. The tunnels run north from the University of Washington to the Maple Leaf portal in north Seattle. The twin bored tunnels were constructed using two EPB TBMs each with an excavation diameter of 6.64 m and supported in a single pass, gasketed segmental lining, 25 cm thick, and an extrados diameter of 6.25 m. Each ring is composed of four full size segments and key and counter key segments. The nominal ring width was 1.5 m, and the universal ring had an overall ring taper of 69.9 mm. The prefabricated segment design concrete strength was 55 MPa, with realized strengths closer to 67 MPa on average. The segments were reinforced with wire mesh with primary D14 reinforcement bars.

The geology of the area through which the tunnels were constructed consists of complex and highly variable interlayered glacial and non-glacial soil deposits. As part of the geotechnical baseline work, the geological units were grouped into engineering soil units (ESU) based on their behavioral characteristics. All tunnel excavation was conducted in the following glacially over ridden ESUs; till and till-like deposits (TLD), cohesionless sand and gravel (CSG), cohesionless silt and fine sand (CSF) and cohesive clays and silts (CCS). Figure 1 shows the variable geological conditions found at the two cross section discussed in this paper.

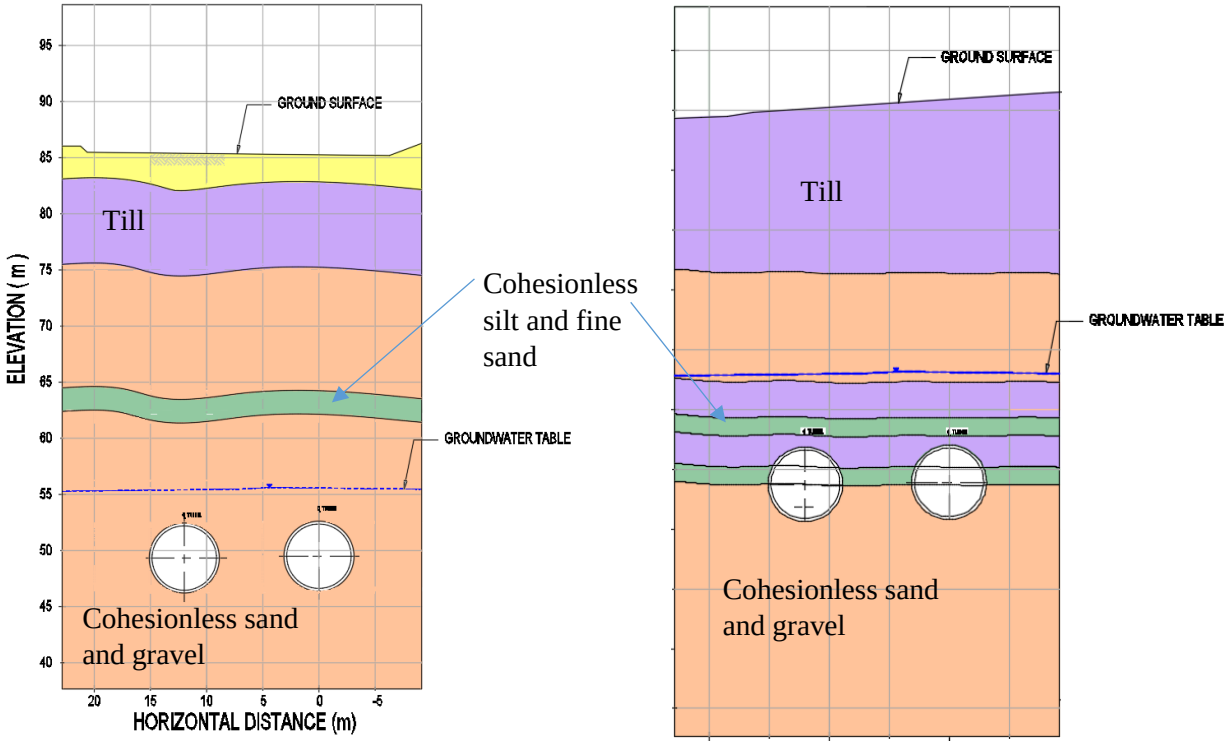

Figure 1. On the left the Northgate link geological cross section 1 at station 1335+00, on the right cross section 2 at station 1327+70

INSTRUMENTATION AND MONITORING

As part of the monitoring program wireless RFID strain gauges were installed in select precast concrete segments (Epel et al. 2018a, Epel. et al. 2018b). Data from two locations or cross-sections are presented in this paper. Within each selected ring, three segments were instrumented – two full-size segments plus a key or counter key. Each instrumented segment was outfitted with a set of two vibrating wire strain gauges welded to the reinforcement cage, one at the intrados and one at the extrados. The strain gauges were installed in a slightly asymmetrical configuration due to limitations in the casting process (Figure 2b). The intrados strain gauge center axis depth from the segment extrados is 58 mm as the strain gauge is installed on #3 rebar (9.5 mm) welded to the underside of the longitudinal 14 mm diameter (i.e., away from the intrados concrete face) rebar welded to the primary reinforcement (14 mm diameter), and minimum clearance is 25 mm. The extrados sister bar was installed on the exterior of the longitudinal reinforcement resulting in a depth of approximately 37 mm for the extrados stain gauge center axis. The strain gages were part of a wireless sensing system developed by Phase IV Engineering (Boulder, Colorado). The layout, implementation and recording program was developed in cooperation between the tunnel contractor JCM Northlink and designer L-7 Services (based in Golden, Colorado). Collection of the strain gauge readings required passing a flat panel RFID reading unit within 30 cm of the concrete surface in the vicinity of the embedded sensor. The monitoring schedule included an initial zero strain reading after the welding of the sister bars, and prior to casting, followed by readings every two weeks after segment installation.

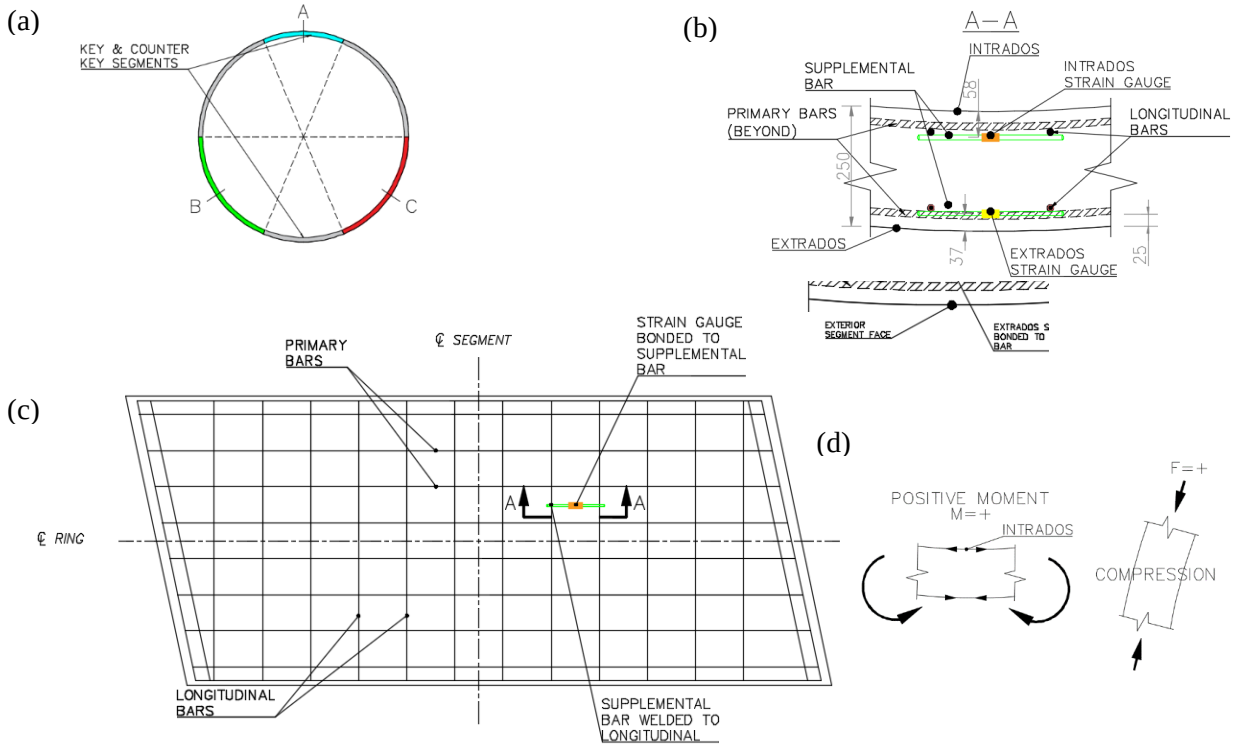

Figure 2. a) Cross section of a typical instrumented ring, with the instrumented segments marked A, B & C. b) Segment cross section at strain gage location (dimensions in mm). c) Strain gage location on a typical segment plan view d) Sign convention for bending moments and thrust force

The orientations of the strain gauges allowed measurement of the circumferential strain and interpretation of the stress developed in the pre-cast segments. With known geometry and strain gauge depth, the measurements collected from a set of two strain gauges allowed for the calculation of both thrust forces (hoop forces) and bending moments developed. The sign convention of the thrust forces and bending moments is positive for compressive thrust force, and positive for bending moment when the segment intrados is in tension (Figure 2d). A different arrangement of the instrumented rings was installed at the two cross section presented in this paper (Figure 3). In cross section 1 only two rings were instrumented at the second (SB) tunnel excavated. In cross section 2 one ring was installed at the first tunnel excavated and two rings at the second tunnel excavated.

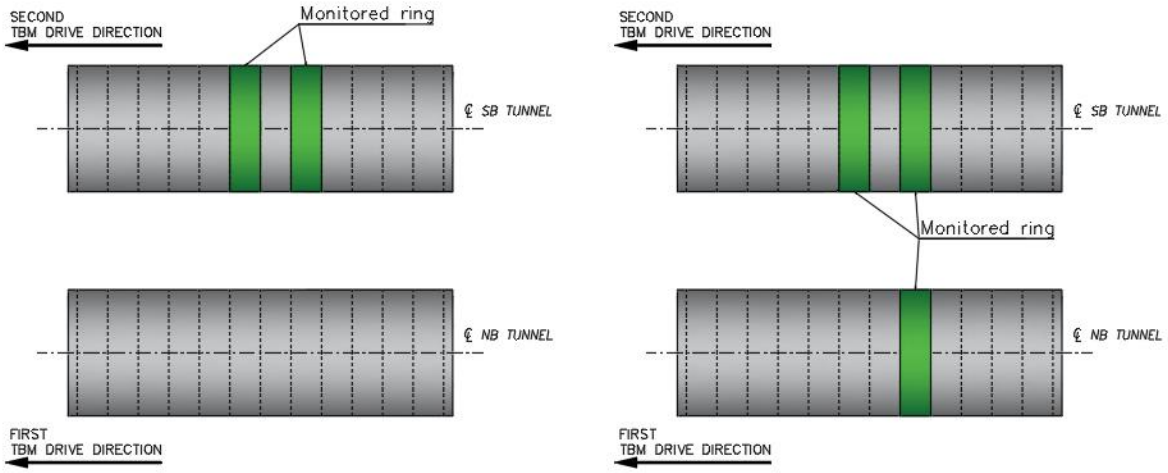

Figure 3. Instrumented rings marked in green at the two cross section, on the left cross section 1 and on the right cross section 2

NUMERICAL MODELING

An accurate prediction of lining forces requires modeling of the tunneling procedure and significant behavioral models including models for: soil constitutive behavior, grout pressure and stiffness, segmental joint rotational behavior, and 3D effects. In this study the soil constitutive model, the segmental joint rotational stiffness, and grout stiffness sensitivity are not investigated. The main purpose of this study is to examine the influence of two common 2D plain strain analysis approaches of the 3D effects of the face of excavation. The first is the 'wished into place' approach, where no pre-convergence or ground relaxation is allowed prior to liner installation. The second approach allows for pre-convergence according to the grout pressure method presented by Moeller (2006). In this study a 2D numerical model is adopted based on the work of Do et al. (2013) and is described in this section.

The 2D modeling was carried out using the finite difference program FLAC 3D. The general configuration of the 2D models is presented in Figure 7 for cross section 1. Each tunnel has an excavation diameter of 6.64 m with an annulus gap of 22.5 cm. The lining is modeled with embedded liner elements with the full thickness of 25 cm. The distance between the tunnel center lines is 12.2 m (1.85 diameters), and the depth to springline is 5.5 and 4.8 diameters. The 2D model size is 124 m in the transverse direction and extends 31 m under the tunnel SL with a total of 8016 elements. Symmetry is not used so

that the influence of twin tunnel excavations can be investigated. The boundary conditions were set as fixed in the horizontal direction at the sides and fixed in both directions at the bottom (figure 7).

The segmental lining is modeled by embedded liner elements connected by double node connection links at each node (Figure 4), to permit the interaction between the host medium (ground), and the structure element. While one side of the element is connected to the surrounding ground, the link at the other side is manipulated to connect the two separate segments. Based on Leonhardt and Reimann (1966), Janssen (1983) developed a simple quantification of the properties for these longitudinal segmental joints. The joints are described in the form of moment-rotation relationship Equations (1) and (2).

$$linear: \left\{\phi = \frac{Mh}{EI} = 12\frac{M}{Eh^2b}\right\} \qquad M < \frac{1}{6}F_n h \qquad \phi < \frac{2F_n}{Ehb} \tag{1}$$

$$non-linear: \left\{\phi = \frac{8F_n}{9bhE\left(\frac{2M}{F_n h}-1\right)}\right\} \qquad M < \frac{1}{6}F_n h \qquad \phi \geq \frac{2F_n}{Ehb} \tag{2}$$

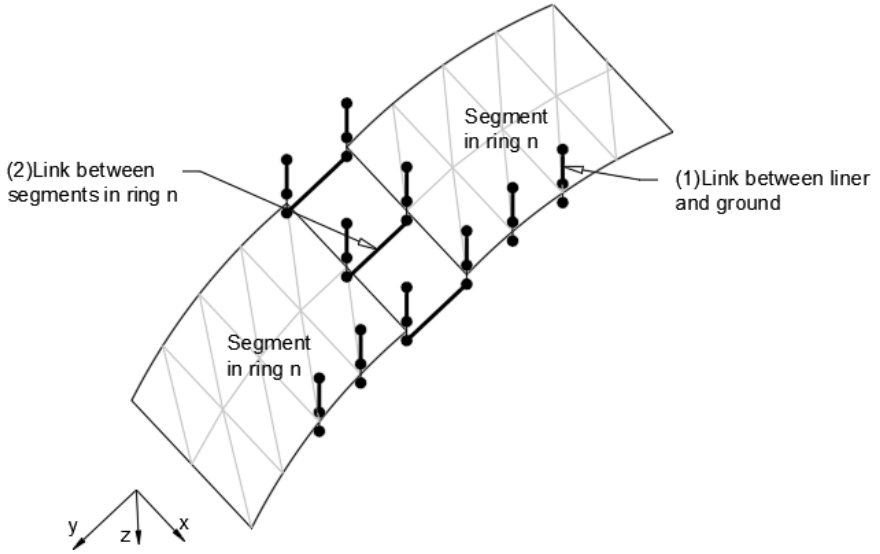

Figure 4. Segmental lining node connectivity concept (after Do et al. 2013)

This behavior of the segmental joints is significantly controlled by the normal force at the joint. With high normal force at the joint and low moments, the joint remains closed with only compression pressure on the entire cross section. However, with high bending moment or small joint thickness, a gap will form when the pressure at the outer/inner side becomes zero, leading to significant additional rotation. The application of this method can be done by a simplified process to determine the values of the spring constants. The simplified procedure used by Do et al. (2013), and Thienert and Pulsfort (2011) requires first to calculate the reference case with full hinge release at the joints. From the average normal force developed in the tunnel lining, the maximum limit bending moment is calculated for an angle rotation ϕ of 0.001 radians, which is assumed as an approximation of the maximum, permissible rotation. Do et al. (2013), and Thienert and Pulsfort (2011) also showed that the segmental joint moment-angular rotation relationship can be simplified by a bilinear model (Figure 5).

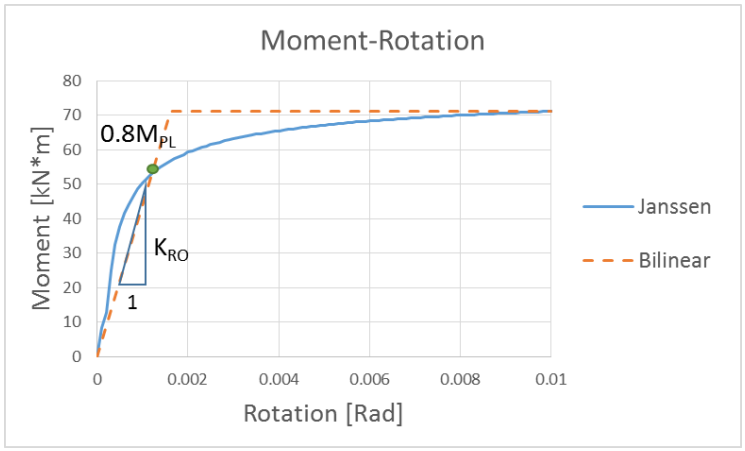

Figure 5. Bending moment – joint rotation relationship of the longitudinal joint

In this study, for the joint rotational stiffness, a bi-linear rotational spring is given to the joints as shown in figure 5. While the translational connections are given a rigid connection as Do et al. (2013) found that the axial and radial stiffness have a negligible effect on the segmental lining behavior.

The grout used in the project reached an average strength of 1.7 MPa in 28 days which correlates to an elastic modulus of 150 MPa according to a study made by Sharghi et al. (2017). In the study presented here the grout is modeled with a time dependent function seen in Figure 6, based on the work of Kasper and Meschke (2004), where the initial stiffness of 8 hours is assumed for fresh grout properties to adjust for the fast gel time of the two-component grout.

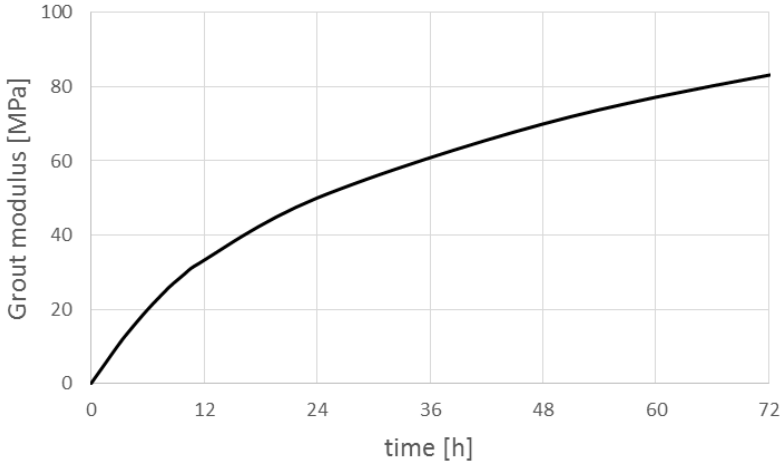

Figure 6. Time-dependent elastic modulus of the grout according a 28 day strength of 150 MPa to Kasper and Meschke (2004)

The use of a non-linear soil constitutive model in pressure balance TBM tunneling is significant, as the ground is subjected to loading-unloading-reloading cycles in changing confinement conditions. The Plastic-Hardening model (Itasca 2009) was adopted in this study, to account for nonlinear stiffness due to the variation in confining stresses and unloading-reloading. The properties used were validated using available triaxial tests and pressuremeter tests.

Modeling the liner-ground interaction with 2D plane strain analysis requires assumptions to simulate the effects of the 3D tunneling process. This is accomplished with the well-known convergence confinement method (CCM) based on the work of Panet (1982), Vlachopoulos and Diederichs (2009), and others. For pressure balance TBM tunneling in non-linear ground behavior an incremental stress reduction procedure is required to build the ground reaction curve (GRC). This is done by the grout pressure method (Moller 2006). The transition from initial geostatic stresses to grout-pressure/machine-pressure state is expressed by Equation 3 (Moller 2006), where σ_0 is the initial normal stress and σ_g is the grout pressure.

$$\sigma = (1 - \lambda)\sigma_0 + \lambda \cdot \sigma_g \tag{3}$$

The normal stress can be given as a function of the initial vertical and horizontal stresses by equation 4 (Moller 2006).

$$\sigma_0 = \sigma_{h0}\, sin^2\, \alpha + \sigma_{v0}\, cos^2\, \alpha \tag{4}$$

The pre-convergence at the location of lining installation can then be obtained according to the longitudinal displacement profile (LDP) of Vlachopoulos and Diederichs (2009) in the following equation.

$$u(x) = u_{max}\left[1 - \left(1 - \frac{u_f}{u_{max}}\right) e^{-\left(\frac{3x}{r_0}, \frac{r_0}{2r_p}\right)}\right] \tag{5}$$

Here, x is the distance from the face and u_f is the radial displacement at the face according to equation 6.

$$u_f = u_{max}\frac{1}{3} e^{-0.15\left(\frac{r_p}{r_0}\right)} \tag{6}$$

The 3D effect of the distance from the face can be simulated by coupling the LDP and GRC and applying a fictitious internal pressure using Equation 4 in a 2D numerical model that will result in the pre-convergence estimated by Equation 5 prior to liner placement.

For the simulation of the construction process in the zero pre-convergence models (wished into place), three stages have been carried out: (1) an initial state of undisturbed ground under gravity conditions (geostatic loading); (2) the removal of the excavation material (6.25 m diameter), installation of the lining, and change of the material in the annular gap to hard grout; and (3) a repeat of stage 2 for the second bored tunnel.

For the simulation of pre-convergence, the CCM was implemented for each tunnel according to the grout pressure method (Moller 2006) before lining installation, followed by modeling the time dependent pressures and properties of the annulus grout summarized in Figure 6. In each pre-convergence model a total of 19 stages were calculated for each tunnel, with 9 pre-convergence stages prior to lining installation, followed by 9 additional calculation stages to account for the annulus grout time dependent behavior. The specific stages are: (Stage 1) the initial state of undisturbed ground; (Stages 2-10) removal of the excavation material and the annulus gap material, incremental reduction of the confinement pressure (increasing λ from 0-0.92 in equation 3) down to the anticipated displacement (corresponding to λ=0.92) at the shield tail 1.6 diameters (10.5 m) behind the tunnel face; (Stage 11) installation of the lining and annulus grout material with fresh grout properties, and application of the grout pressure acting on both the lining and the excavation boundary; (Stage 12) removal of grout pressure; (Stages 13-19) time dependent hardening of the annulus grout to its final 28 day strength. After the completion of the first tunnel excavation sequence the same staging sequence is applied for the second tunnel.

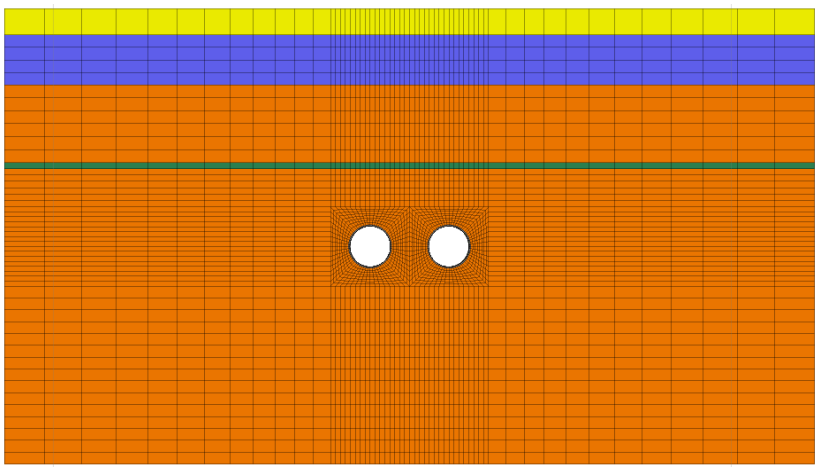

Figure 7. The 2D model used for the calculation of cross section 1

RESULTS AND DISCUSSIONS

Cross section 1 included two instrumented rings installed in the second tunnel (SB) excavated. Strain gage measurement collection began 63 days after ring installation. Strain gage measurement continued for 500 days after SB tunnel construction at this cross section. While in cross section 1 strain monitoring was done only at the second tunnel, in cross section 2 both tunnels were monitored; one ring in the NB tunnel that was excavated first, and two rings at the SB tunnel that was excavated second. Unfortunately, data collection began 50 days after the second tunnel passed the monitored cross section. Strain gage measurement continued for 390 days beyond SB tunnel construction at this cross section. The values shown in Figures 7 and 8 are taken at 55 days after the second TBM pass having a distance greater than 20 diameters and hardened annulus grout.

Force development in the first tunnel

Figures 8a and 8b show results from the two analysis approaches of the first tunnel at cross section 1. For each numerical calculation two stages are displayed: the first stage is after the excavation and support of only a single tunnel, and the second stage is after the excavation and support of the second tunnel, constructed at a distance of 2D between axes. With no instrumented rings in the first tunnel excavated, comparing only between the two approaches, a significant increase of bending moments and thrust forces is seen in the model accounting for pre convergence as a result of the second tunnel excavation. However, in the ‘wished into place’ model a negligible change in bending moment and a slight change in thrust force is observed. While the difference in maximum absolute value of bending moment between the two methods at the final stage is only 2%, the thrust force estimated when pre-convergence is allowed is lower by about 35% from the wished into place approach. Figure 9b shows a similar thrust force behavior in cross section 2 between the two approaches as observed in cross section 1. Figure 9b also shows a much better agreement between the field measurements and the approach allowing pre-convergence. Despite the good agreement between the thrust force measurements and the estimated forces using the pre-convergence approach, the bending moments measured fit the wished into place prediction better (Figures 9a).

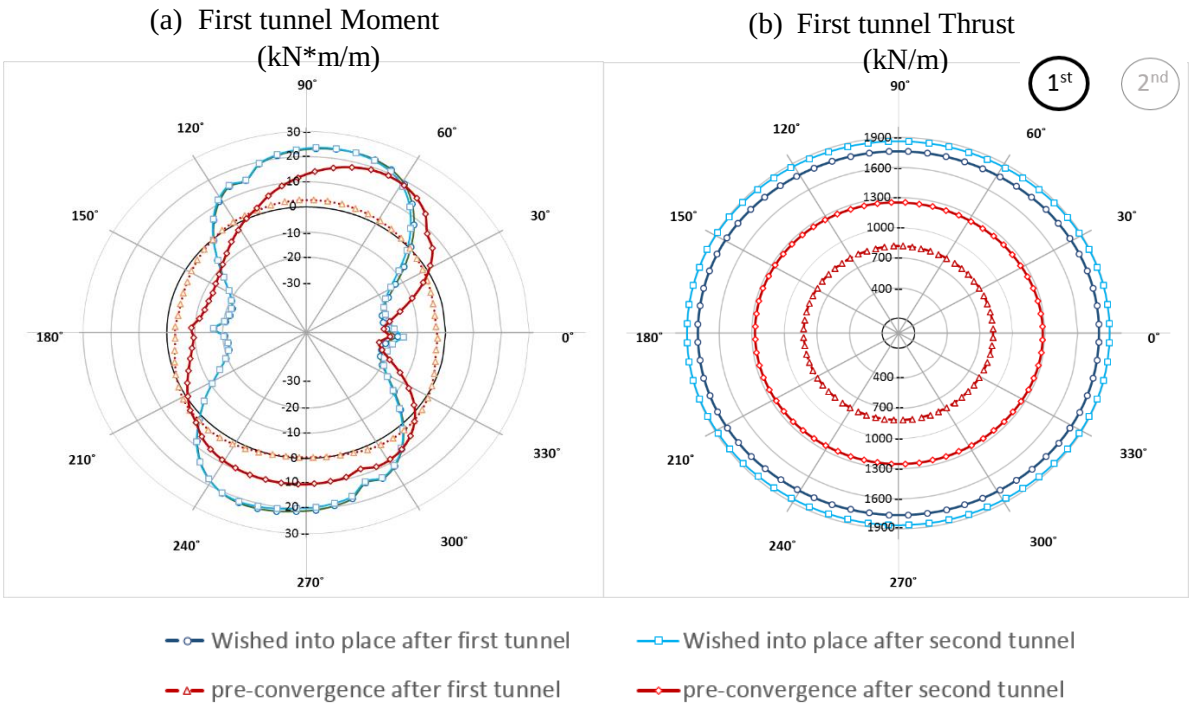

Figure 8. Cross section 1 in the first tunnel: (a) Bending moment (kN-m/m) and (b) Thrust force (kN/m) diagrams after first tunnel excavation, and after to second tunnel excavation

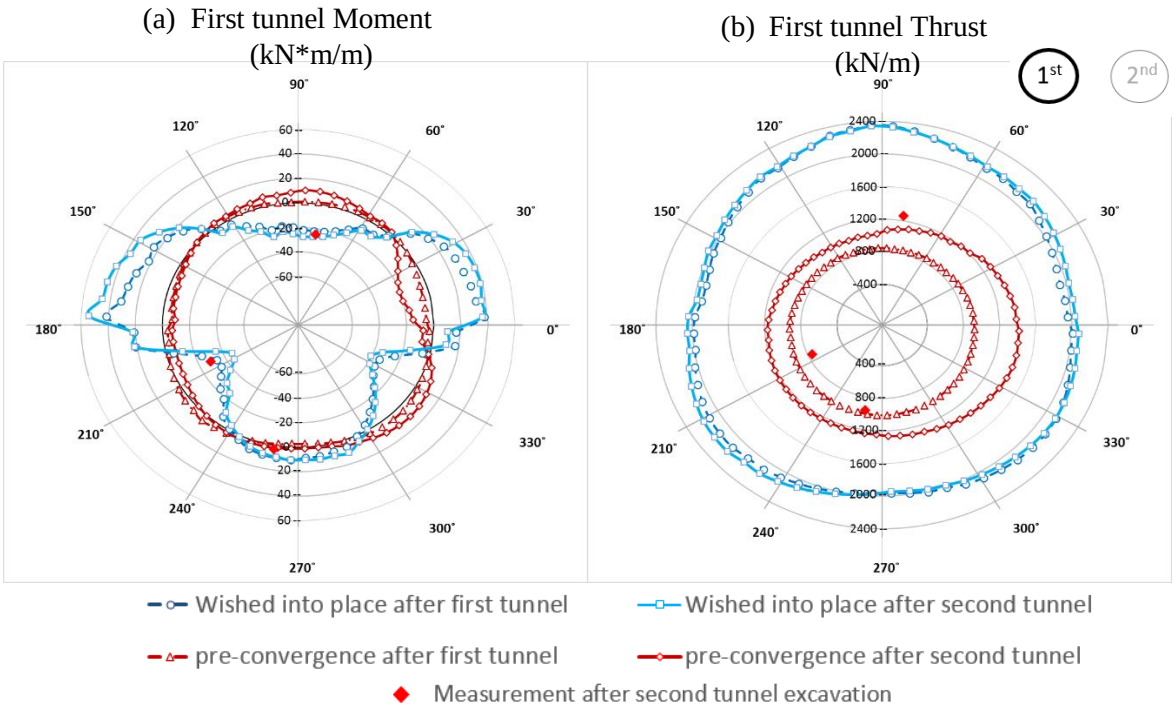

Figure 9. Cross section 2 in the first tunnel: (a) Bending moment (kN-m/m) and (b) Thrust force (kN/m) diagrams after first tunnel excavation, and after to second tunnel excavation

Force development after second tunnel excavation

In both cross sections liner loads were measured at the second tunnel (SB) excavated. In Figure 10b, it can be observed that the measured thrust forces at cross section 1, are in better agreement with the predicted forces using the pre-convergence approach, and are within an error of 5-30%. Where in the 'wished into place' approach the predicted values differ by 50-100%. Figure 11b showing the thrust forces at cross section 2 match the behavior observed in cross section 1 (figure 10b) with the measured force in good agreement with the pre-convergence model which are also lower by about 50% from the 'wished into place' approach. Similar to what was observed in the first tunnel at cross section 2, the bending moments at both cross section 1 (Figure 10a) and cross section 2 (Figure 11a) good agreement with the 'wished into place' approach.

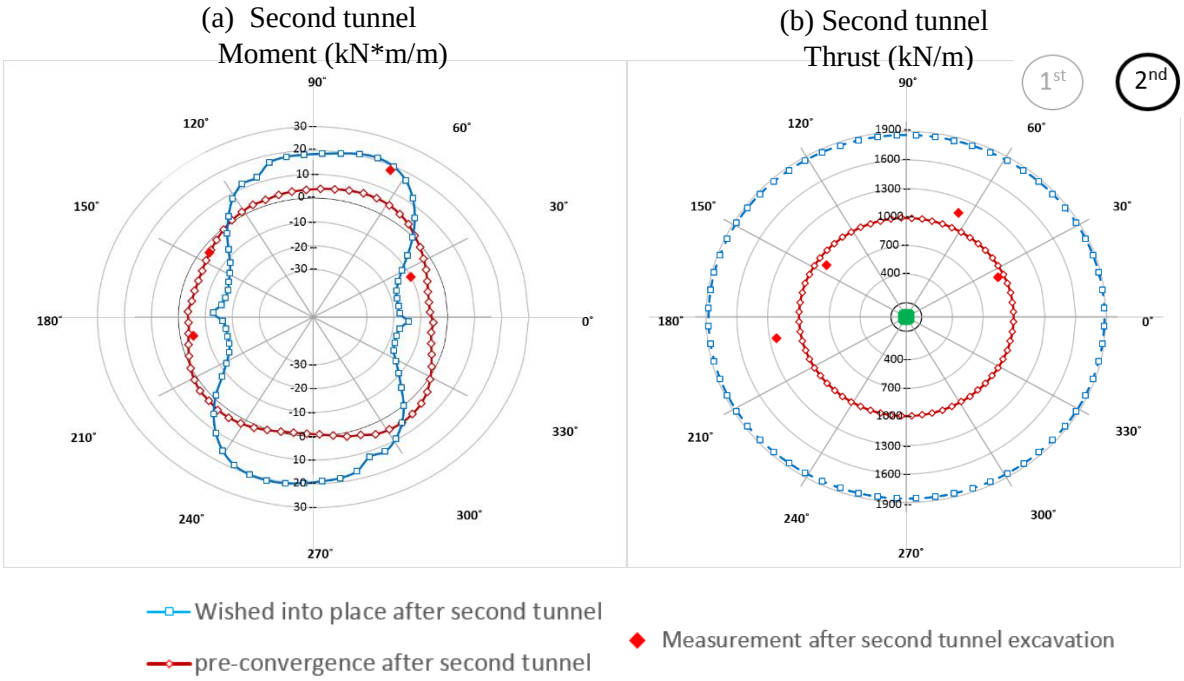

Figure 10. Cross section 1 in the second tunnel: (a) Bending moment (kN-m/m) and (b) Thrust force (kN/m) diagrams

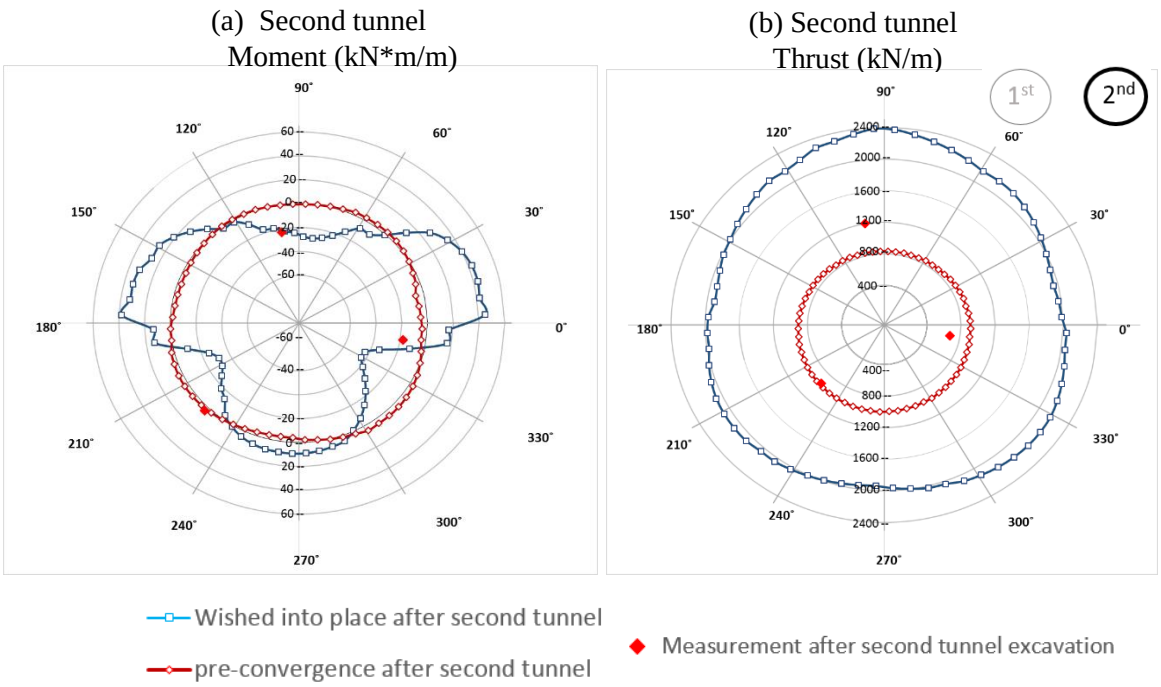

Figure 11. Cross section 2 in the second tunnel: (a) Bending moment (kN-m/m) and (b) Thrust force (kN/m) diagrams

CONCLUSIONS

This study presented a comparison of 2D plane strain numerical calculations with and without the use of convergence-confinement method (CCM) principles. The results of the analysis are validated with bending moment and thrust force from field strain gage measurements during the Northgate Link project in Seattle. From this series of analysis the following conclusions are drawn:

- Thrust forces predicted using the no pre-convergence approach (wished into place) results in forces higher than the forces measured by 50-150%, while when accounting for pre-convergence (CCM) the thrust forces estimated are with 20% of the measured force in average.
- Contrary to the prediction of thrust forces, bending moments predicted using the no pre-convergence approach (wished into place) resulted in better agreement compared to the very low bending moments predicted when accounting for pre-convergence (CCM).
- The calculation of the internal lining forces without taking into account pre-convergence is commonly perceived as conservative in that it typically results in higher bending moments and thrust forces. However, the measured combination of a high bending moment with low axial force in fact finds this approach can be unconservative, and in some situations can lead to exceeding the thrust-moment (N-M) capacity envelope.

Although some may believe that a simplified analysis that neglects the effects of relaxation is a more conservative design approach, this may not be the case. Combining the discussed approaches with different expected face pressures should be used to build the loading cases used in the design of segmental pre-cast concrete linings. This should reduce the uncertainty and potentially allow lower safety factors for design.

REFERENCES

Do, N.A., Dias, D., Oreste, P., Djeran-Maigre, I. 2013. 2D numerical investigation of segmental tunnel lining behavior. Tunneling and Underground Space Technology, 37 (2013), pp. 115-127, 10.1016/j.tust.2013.03.008

Einstein, H.H. and Schwartz, C.W. 1979. "Simplified analysis for tunnel supports". Journal of the Geotechnical Engineering Division, 499-517.

Epel, T., Mooney, M., Gutierrez, M., Braun, K., DiPonio, M., Long, N. 2018a. Analysis Methodologies Comparison of Estimated and Measured Precast Segment Liner Loads Developed During Construction of twin EPB TBM Tunnels in Seattle. World Tunnelling Conference 2018.

Epel, T., Mooney, M., Gutierrez, M., Braun, K., DiPonio, M., Long, N. 2018b. Ground-Liner Interaction during Seattle Northgate Link Cross-Passage. Construction North American Tunneling Conference 2018.

Frank, G., Hagan, B., Sandell, T., Gharahbagh, E.A., Willis, D., Diponio, M.A., Cowles, B. 2015. Preparation for Tunneling, Northgate N125 Project in Seattle, Washington, Rapid Excavation and Tunneling Conference 2015.

Itasca. 2009. FLAC Fast Lagrangian Analysis of Continua, Version4.0. User's manual. FLAC Fast Lagrangian Analysis of Continua, Version 4.0. User's manual.

Janssen, P. 1983. Tragverhalten von tunnelausbauten mit gelenktubbings, Ph.D. Thesis Technischen Universitat Carolo-Wilhelmina, Braunschweig, December 1983

Kavvadas, M., Litsas, D., Vazaios, I., Fortsakis P. 2017. Development of a 3D finite element model for shield EPB tunneling Tunn. Undergr. Space Technol., 65, pp. 22-34

Lambrughi, A., Medina Rodríguez, L., Castellanza, R. 2012. Development and validation of a 3D numerical model for TBM–EPB mechanised excavations. Comput. Geotech. 40, 97–113.

Leonhard, F., & Reimann, H. 1966. Betongelenke. Der Bauingenieur, 41, 49-56.

Moller, S. 2006. Tunnel Induced Settlements and Structural Forces in Linings, PhD Thesis, Universitat Stuttgart.

Muir Wood A. 1975. "The circular tunnel in elastic ground". Géotechnique 25(1), 115-127.

Panet M., Guenot A. 1982. Analysis of convergence behind the face of a tunnel. Proceedings, International Symposium Tunnelling'82, IMM, London, pp 197–204

Thienert, C., Pulsfort, M., 2011. Segment design under consideration of the material used to fill the annular gap. Geomechanics and Tunneling 4, 665–679.

Vlachopoulos N., Diederichs M.S. 2009. Improved longitudinal displacement profiles for convergence confinement analysis of deep tunnels. Journal of Rock mechanics and Rock Engineering, vol 42, Number 2, April 2009. pp 131–146